Joint free pavements made with HPFRC

Computational Modelling of Concrete and Concrete Structures – Meschke, Pichler & Rots (Eds)

Joint free pavements made with HPFRC

Alessandro P. Fantilli, Nicholas S. Burello & Masood Khan
Politecnico di Torino, Torino, Italy

Giovanni Volpatti
CEMEX Innovation Holding AG – Brügg Branch, Brügg, Switzerland

Jorge C. Diaz Garcia
CEMEX LATAM Holding AG – Swiss Branch, Brügg, Switzerland

Davide Zampini
CEMEX Innovation Holding AG, Zug, Switzerland

ABSTRACT: Concrete has been widely used in the construction of roads, highways, industrial floors and pavements since early twentieth century. Construction methods generally include placement of joints at specific distances to control the cracking phenomenon. The latter is due to the development of tensile strains caused by the shrinkage of concrete and by environmental factors, such as temperature gradient. However, joints result in reduced load carrying capacity, local failure, and pavement damage. To reduce the number of joints, the fracture toughness of concrete can be enhanced by adding fibers. As the models available for conventional fiber-reinforced concrete (FRC) cannot be extended to high-performance fiber-reinforced concrete (HPFRC), the aim of this work is to describe a new model to design HPFRC joint free slabs. Specifically, a composite cross section made of soil and concrete, which is subjected to imposed strains, is modelled through the Colonnetti's theory of elastic coactions. In this way, not only the effect produced by concrete shrinkage but also the nonlinear response of HPFRC in the strain hardening stage are taken into account. For given maturity curves, crack does not appear if the maximum tensile strain provided by the model is lower than the strain that produces localization in HPFRC.

1 INTRODUCTION

Nowadays, reinforced concrete is the most used building material, especially in structures and infrastructures. Focusing on pavements, concrete is almost the only alternative to asphalt, and the first guidelines for the design of concrete pavements were introduced about 30 years ago (AASHTO 1993). Afterwards, several guidelines were also proposed (Choi et al. 2005; Rasmussen et al. 2009; Roesler et al. 2016; Söderqvist 2006).

Although concrete slabs guarantee longer term service life and can be easily built, a specific attention is required during the first days of curing. Indeed, due to the shrinkage phenomenon and to the low strength in tension, concrete is prone to cracking at early age. More precisely, when applied stress overcomes the tensile strength, concrete fails and crack growths. It can occur just after casting, when strength increases at a slower rate than the constrained stresses induced by the reduction of volume.

As cracks can compromise both durability and functionality of pavement, contraction joints are frequently used to control the cracking phenomenon (FHA 2019). In practice, the upper side of the slabs is sawn at regular intervals during the first hours after casting.

Nevertheless, joints generate several problems to the pavement in service. Traffic movements can damage the joint (joint-edge chipping and cracking) and facilitate the penetration of aggressive chemicals, which in turn affect the durability of pavements. For these reasons, jointless pavements, also made with fiber reinforced concrete, have been proposed (ChunPing et al. 2015; Larrard et al. 2011; Zhang et al. 2013). In fact, several studies have shown that the addition of fibers, either steel or polymeric, improves the mechanical properties in tension, and controls the widening of cracks (Tehmina et al. 2014; Yoo et al. 2018). At early age, experimental results show that the presence of $0.2 \div 0.3\%$ of nylon fibers may reduce the effect of drying shrinkage (up to 75%) in a cementitious matrix (Choi et al. 2011). Furthermore, the performances improve when high performance fiber reinforced concrete (HPFRC) is used to cast thin concrete pavements, even in the case of instant repairs or quick renewal of roads (Burger 2010; Hachiya et al.

DOI 10.1201/9781003316404-86

2006, R. 2009). As HPFRC shows a strain-hardening behavior (Graybeal 2016) before reaching the localization of tensile strain (Ramadoss 2008; Savino et al. 2018), the fibers may completely substitute the conventional reinforcement, and reduce/eliminate the presence of joints.

For instance, Destrée et al. (2016) discussed the main parameters of concrete shrinkage and provided a model for the analysis of slab made of FRC (see Figure 1). It is based on the classical tension stiffening equations of RC structures, and includes the bond slip mechanisms between soil and FRC and between fiber and matrix, and the fracture mechanics of the matrix in tension.

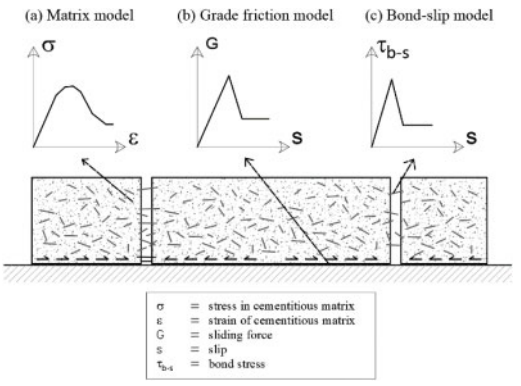

Figure 1. Mechanical behavior of cracked fiber-reinforced cementitious composite (Destrée et al. 2016): (a) stress-strain relationship of the cement-based material; (b) bond-slip model between FRC and soil; (c) bond-slip model of the fiber within the matrix.

Although the model can be used to design jointless slabs using steel fibers, the application cannot be extended to HPFRC, because, for this cement-based material, the strain localization in tension, $\varepsilon_{c,cp}$, does not occur at the first cracking, $\varepsilon_{c,cr}$ (see Figure 2b). Accordingly, a new model, able to predict the mechanical behavior of slabs on grade is proposed. More precisely, a composite cross-section made of concrete and elastic soil (see Figure 3), and subjected to the imposed strain ε_{sh} (sh = shrinkage), is analysed. The proposed model calculates the internal states of stress and strain by means of the Colonnetti's theory of elastic coactions (Colonnetti 1950), when material properties are known at every stage of curing. The model works within Stage I (i.e., in absence of strain localization) and can be applied also in the cases of conventional concrete and FRC, in which $\varepsilon_{c,cr} = \varepsilon_{c,cp}$ (Figure 2a).

2 PROPERTIES OF MATERIALS

The model analyzes slabs on ground during the curing stage, just after casting. To evaluate the state of stress and strain in this scenario, it is necessary to know the mechanical properties of concrete, including shrinkage, at any time. However, each parameter (e.g., shrinkage strain, tensile strength, compressive strength, etc.) shows different rate of development after casting.

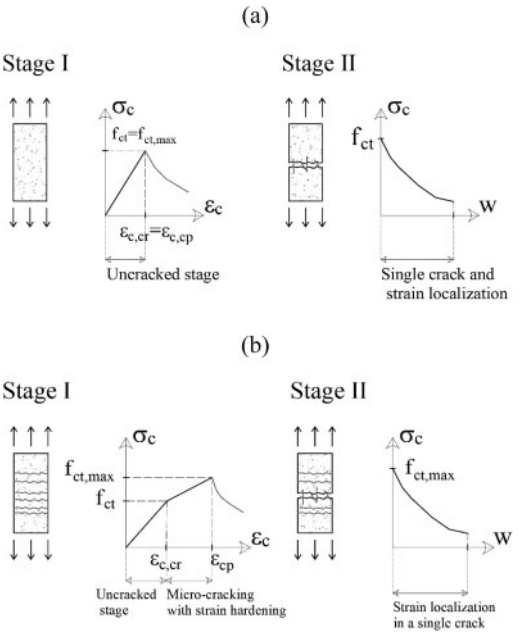

Figure 2. Tensile behavior of (a) conventional FRC and (b) HPFRC.

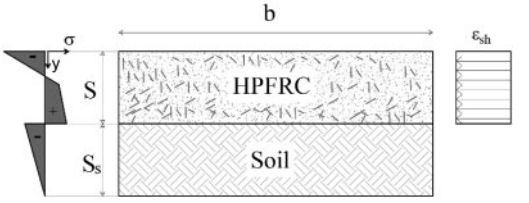

Figure 3. Composite cross-section analyzed by the proposed model, in the case of uniform shrinkage strain ε_{sh}.

2.1 *Mechanical performances of concrete and soil*

HPFRC has a strain hardening response in tension (as depicted in Figure 2b) and a linear elastic behavior in compression. The parameters of a possible stress-strain relationship are described by exponential equations (Eurocode 2 1-1 1992; fib Model Code 2010; ACI 209R-92 1997). However, tensile strength tends to increase more rapidly than the compressive strength (Bentur 2003).

Some studies (Boshoff 2012; Combrinck et al. 2019; Hammer et al. 2007; Roziere et al. 2015) defined the tensile strain capacity of concrete at early age, which reaches the minimum during the setting time (up to 10 hours) and before early hardening (see Figure 4). This is due the fact that a significant increase of

the elastic modulus occurs earlier than the increment of the tensile strength. For this reason, two types of analyses are carried out after casting:

- short term analysis (STA), from 2 hours to 96 hours;
- long term analysis (LTA), from 4 days to 28 days.

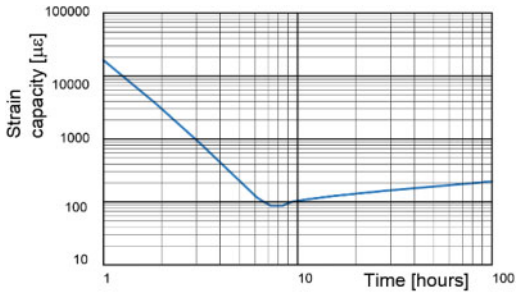

Figure 4. Tensile strain capacity *vs*. time (Boshoff 2012).

In both the cases, the equations provided by Eurocode 2 are taken into consideration. Specifically, compressive strength of concrete, at various ages, may be estimated as follows:

$$f_{cm}(\tau) = \beta_{cc}(\tau) \cdot f_{cm} \tag{1}$$

$$\beta_{cc}(\tau) = exp\left\{ s\left[1 - \left(\frac{28}{\tau} \right)^{1/2} \right] \right\} \tag{2}$$

where $f_{cm}(\tau)$ = mean concrete compressive strength at time τ; f_{cm} = mean compressive strength at 28 days; $\beta_{cc}(\tau)$ = coefficient which depends on τ; and s = coefficient that depends on the type of cement.

As a first approximation, the value of the tensile strength with time, $f_{ctm}(\tau)$, is given by:

$$f_{ct}(\tau) = (\beta_{cc}(\tau))^{\alpha} \cdot f_{ctm} \tag{3}$$

where f_{ctm} = mean tensile strength at 28 days of curing; and $\alpha = 1$ when $\tau < 28$ days.

Focusing on the stiffness, the variation of the modulus of elasticity with time, $E_{cm}(\tau)$, is:

$$E_{cm}(\tau) = \beta_{cc}(\tau)^{0.3} E_{cm} \tag{4}$$

where E_{cm} = modulus of elasticity at 28 days.

Tensile strain at cracking can be calculated by using the modulus of elasticity in compression, $E_{cm}(\tau)$, and the tensile strength $f_{ctm}(\tau)$:

$$\varepsilon_{c,cr}(\tau) = {}^{f_{ct}(\tau)}/_{E_{cm}(\tau)} \tag{5}$$

To take into account the results of previous studies (Boshoff 2012; Combrinck et al. 2019; Hammer et al. 2007; Roziere et al. 2015), in the case of STA, the tensile strain capacity is calculated by means of a suitable correction:

$$\varepsilon_{c,cr}(\tau) = \varepsilon(\tau) \cdot \frac{\varepsilon_{c,cr}(\tau = 96h)}{\varepsilon(\tau = 96h)} \tag{6}$$

where $\varepsilon(\tau) = \varepsilon(\tau = 96\,\text{h})$ = tensile strain at first cracking, calculated at $\tau = 96$ h, respectively on the function drawn in Figure 4; and $\varepsilon_{c,cr}$ ($\tau = 96$ h) = strain at first cracking calculated through Eq.(5).

In other words, the tensile strain at first cracking is calculated by scaling the curve reported in Figure 4 (Boshoff, 2012), with respect to the value computed at 96h (Eurocode 2 1-1 1992). Young's modulus is consequently updated with respect to the new value of tensile strain capacity by means of Eq. (5). Ultimate tensile strain (i.e., $\varepsilon_{c,cp}$ in Figure 2b) and the slope of the hardening branch can be similarly calculated.

The soil, assumed as an aged material, is characterized by an elastic modulus, E_{to}, at the interface with the slab. It linearly increases with the depth according to the coefficient K_t, as shown in Figure 5. Hence, for a given thickness, S_S, of the soil, the average value of the elastic modulus is given by:

$$E_t\left(z = \frac{S_S}{2}\right) = E_{t0} + \frac{K_t \cdot S_s}{2} \tag{7}$$

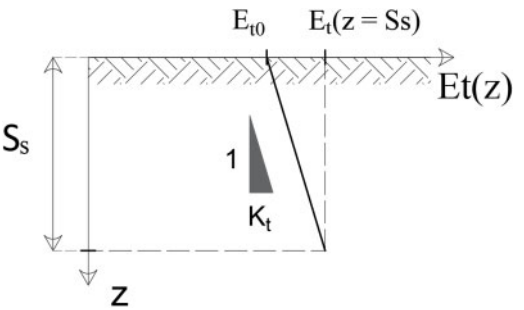

Figure 5. The Young's modulus of soil.

2.2 *Shrinkage model*

Focusing on the curing of concrete, several studies have been carried out in the last years. The shrinkage strain ε_{cs} is composed by the drying, ε_{cd}, and the autogenous, ε_{ca}, contributions:

$$\varepsilon_{cs}(\tau) = \varepsilon_{cd}(\tau) + \varepsilon_{ca}(\tau) \tag{8}$$

Drying shrinkage strain develops slowly, since it is a function of the migration of the water through the hardened concrete. As autogenous shrinkage increases during the hardening of concrete, a major part of ε_{ca} develops in the early days, as illustrated in Figure 6a, where the two components of shrinkage are plotted as a function of concrete aging (Gribniak et al. 2011).

Zhang et al. (2003) noted that most of the total shrinkage in high-strength concrete can be attributed to autogenous shrinkage (see Figure 6b), rather than drying shrinkage. Whereas, due to the higher water-binder ratio, drying shrinkage is dominant in normal concrete (Yoo et al. 2018).

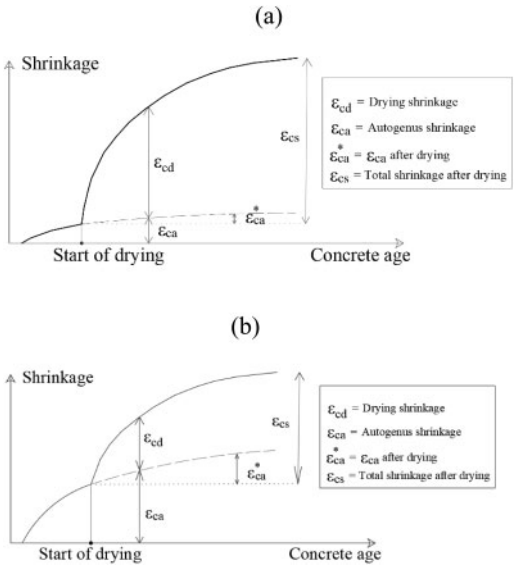

Figure 6. Shrinkage strain components in (a) normal and (b) high-strength concrete.

Gardner & Lockman (2001) provided the GL-2000 model, which can be applied to conventional concrete having the water-cement ratio within the range 0.4–0.6, and a compressive strength lower than 82 MPa (at 28 days). Another model was proposed by Bazant & Baweja (2001). It is called B3 Model and shows very low coefficient of variations, if compared with the results provided by ACI209R (1997) and Eurocode 2 1-1 (1992). In the latter, used herein for the structural analysis, the drying shrinkage strain with the time can be calculated as follows:

$$\varepsilon_{cd}\,(t) = \beta_{ds}\,(\tau, \tau_s) \cdot k_h \cdot \varepsilon_{cd,0} \tag{9}$$

where k_h = coefficient depending on the notional size, and:

$$\varepsilon_{cd,o} = 0.85\left[(220 + 110 * \alpha_{ds1}) * exp\left(-\alpha_{ds2}\frac{f_{cm}}{f_{cmo}}\right)\right] * 10^{-6} * \beta_{RH} \tag{10}$$

$$\beta_{RH} = 1.55\left[1 - \left(\frac{RH}{RH_o}\right)^3\right] \tag{11}$$

$$\beta_{ds}\,(\tau, \tau_s) = \frac{(\tau - \tau_s)}{(\tau - \tau_s) + 0.04\sqrt{h_o^3}} \tag{12}$$

In these equations, $f_{cmo} = 10$ MPa; α_{ds1} and α_{ds2} = coefficients depending on the type of cement; RH = ambient relative humidity (%); RHo = 100%; τ_s = age of concrete (days) at the beginning of drying shrinkage (or swelling); and h_0 = notional size of the cross-section.

The autogenous strain can be calculated as:

$$\varepsilon_{ca}\,(t) = \beta_{as}\,(t)\,\varepsilon_{ca}\,(\infty) \tag{13}$$

where:

$$\varepsilon_{ca}\,(\infty) = 2.5\,(f_{ck} - 10)\,10^{-6} \tag{14}$$

$$\beta_{as}\,(t) = 1 - exp\left(-0.2t^{0.5}\right) \tag{15}$$

The maximum shrinkage strains computed with the previous formulae can vary between 300 and 900 με. However, some researchers (Al-Saleh 2014; Gűneyisi et al. 2014; Yoo et al. 2014; Zhang et al. 2013) suggested an increment of the upper bound, in order to maximize the structural effect of shrinkage on the slabs on ground. Moreover, also the distribution within the thickness of a slab needs to be better investigated. For instance, Rasmussen & McCullough (1998) assumed a linear distribution, in which the full shrinkage strain appears on the surface of the concrete pavement, whereas zero shrinkage is at the mid-depth of the slab. Heath & Roesler (1999) measured the distribution of drying shrinkage by installing strain gauges at different depths of a full-scale slabs on grade. They observed a remarkable difference of shrinkage strain on the top and the bottom of the slab. Thus, shrinkage strain cannot be neglected also on the bottom surface, but, at the same time, it cannot be equal to that on the top. More recently, a new model (Tiberti et al. 2018) assumes 100% of total shrinkage, calculated through Eq. (8), on the free surface. Then, a linear decrement of the drying shrinkage strain is assumed in the rest of the cross-section (it is 50% or 75% lower on the bottom surface).

3 A NEW MODEL FOR SLABS ON GROUND

Referring to the composite cross-section depicted in Figure 3, and made by HPFRC and soil, a new algorithm for measuring the effect of shrinkage of the cement-based material can be developed. To be on the safe side, the stress in the HPFRC is maximized by assuming the existence of the perfect bond between the two layers. Indeed, if a slip between HPFRC and soil exists, both strain and stress reduce in the upper layer.

According to Figure 3, the geometrical input data of the problem are S (= thickness of the slab), S_S (= thickness of the soil), and b (= width of both slab and underlying soil). If the whole cross-section resists to the external actions, the soil can be considered as the steel reinforcement in a reinforced concrete cross-section. After casting, the only load applied on the slab is the shrinkage, which can be considered as imposed strain acting in the concrete layer. Consequently, both stresses and strains in the composite cross-section of Figure 3 can be calculated by using the Colonnetti's theory of elastic coactions (Colonnetti, 1950).

Obviously, the elastic properties of the HPFRC layer vary with the time, therefore, at a fixed time $\tau > 0$, the homogenized geometrical parameters of the composite cross-section are calculated:

$$E_o = E_c(\tau) \tag{16}$$

$$A_o = \frac{E_c}{E_o} \cdot S \cdot b + \frac{E_t}{E_o} \cdot S_s \cdot b \tag{17}$$

$$Y_G = \frac{S_{x0}}{A_0} = \frac{b \cdot s\left(\frac{S}{2} + S_s\right) + \frac{E_t}{E_c} \cdot b \cdot \frac{S_s^2}{2}}{A_0} \tag{18}$$

$$Ix_0 = \left[\frac{bS^3}{12} + b \cdot S\left(\frac{S}{2} + S_s - Y_G\right)^2\right] + \left[\frac{bS_s^3}{12} + b \cdot S_s\left(\frac{S_s}{2} - Y_G\right)^2\right]\frac{E_t}{E_c} \tag{19}$$

where, E_o = Young's modulus of elasticity used to homogenize the cross-section; A_o = homogenized area of the cross-section; Y_g = ordinate of the centroid; S_{xo} = homogenized static moment; and I_{x0} = homogenized moment of inertia.

Assuming that plane section remains plane, the state of stress in concrete ($\sigma_{z,c}$) and soil ($\sigma_{z,s}$) are orthogonal to the Z direction (see Figure 3). They can be calculated as:

$$\begin{cases} \sigma_{z,c} = E\,(\lambda + \mu_x \cdot y - \varepsilon_{im}) & if\ 0 \le y \le S \\ \sigma_{z,s} = E\,(\lambda + \mu_x \cdot y) & if\ S \le y \le S_s \end{cases} \tag{20}$$

where, y = ordinate of the point with respect to the intrados; ε_{im} = imposed strain (in this case, t is due to shrinkage); λ = total axial deformation; and μ_x = in plane total curvature.

The strain parameters (i.e., λ and μ_x) are the sum of the elastic contribution, due to the external explicit actions (i.e., λ_{el} and μ_{el}), and of the effect produced by imposed strain (λ_{pl} and μ_{pl}). As no external loads are applied (i.e., $\lambda_{el} = \mu_{el} = 0$) the total strain parameters are calculated as follows:

$$\lambda = \lambda_{tot} = \lambda_{el} + \lambda_{pl} = \frac{1}{A_0}\int_{Ac}\frac{E_c}{E_c} \cdot \varepsilon_{im} dA \tag{21}$$

$$\mu_x = \mu_{tot,x} = \mu_{el} + \mu_{pl} = \frac{1}{A_0}\int_{Ac}\frac{E_c}{E_c} \cdot \varepsilon_{im} \cdot y dA \tag{22}$$

However, when the non-linear stage of the cementitious matrix is reached (i.e., $\varepsilon_{c,cr} \le \varepsilon \le \varepsilon_{cp}$ in Figure 2b), Eqs.(18)–(19) are not valid.

Nevertheless, according the Colonnetti's theorem (Colonnetti 1950), nonlinear contributions can be taken into account by introducing suitable imposed strain, ε_{nl}, as shown in Figure 7 (where the subscripts "E" = "elastic" and "R" = "real law" indicate the type of stress calculation, respectively). In practice, for a given ε, the linear stress-strain relationship is translated up to the real relationship through ε_{nl}:

$$\varepsilon_{nl} = \frac{E \cdot \varepsilon - \sigma(\varepsilon)}{E} \tag{23}$$

Finally, the state of stress can be calculated with Eqs.(21)–(22) by assuming $\varepsilon_{im} = \varepsilon_{sh} + \varepsilon_{nl}$.

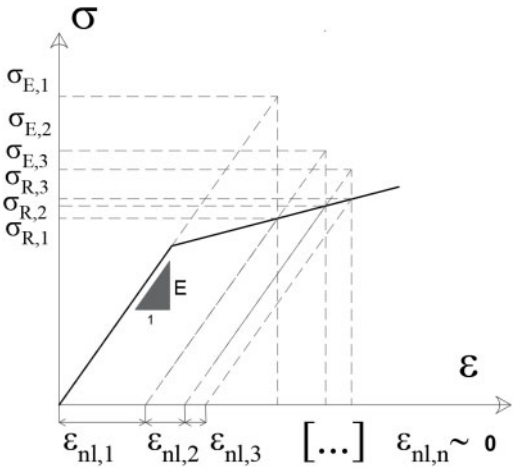

Figure 7. Effect of nonlinear behavior of the constitutive law and calculation of the ε_{nl}.

As ε_{nl} has to be continuously updated, an iterative procedure for the calculation of the states of stress and strain is introduced. The iterations end when the difference between two consecutive values of ε_{nl} is negligible (i.e., when two consecutive states of stress are mathematically coincident).

If the strain in each point of the cross-section is lower than the strain at beginning of strain localization:

$$\varepsilon(y, \tau) \le \varepsilon_{c,cp}(\tau) \quad 0 \le y \le S \tag{24}$$

macrocracks do not appear (or crack width is much lower than the admissible values). In these cases, joints are not necessary.

As tensile stresses in the soil are not allowed, the thickness S_S must be iteratively changed until only compressive stresses are present in the soil (see Figure 3). In other words, the thickness of the soil substrate is not input of the problem. In this way, the whole procedure is composed by the two encapsulated iterative parts shown in Figure 8.

4 NUMERICAL RESULTS

The procedure previously described is herein applied in two different slabs: slab_1 and slab_2. In both the cases, the thickness is the same (S = 100 mm), whereas the mechanical parameters of soil are summarized in Table 1.

The slabs are made with different types of concrete, normal concrete (C30/37) in the slab_1, and HPFRC in slab_2, whose mechanical properties are illustrated in Table 2. The properties of C30/37 are those suggested by Eurocode 2 1-1 (1992) and measured at 28 days. On the contrary, the properties of HPFRC have been provided by a building material supplier, and concern a product available on the market (Esser et al. 2015).

The model computes the states of stress and strain in both the slabs under the hypothesis of a curing at 20°C

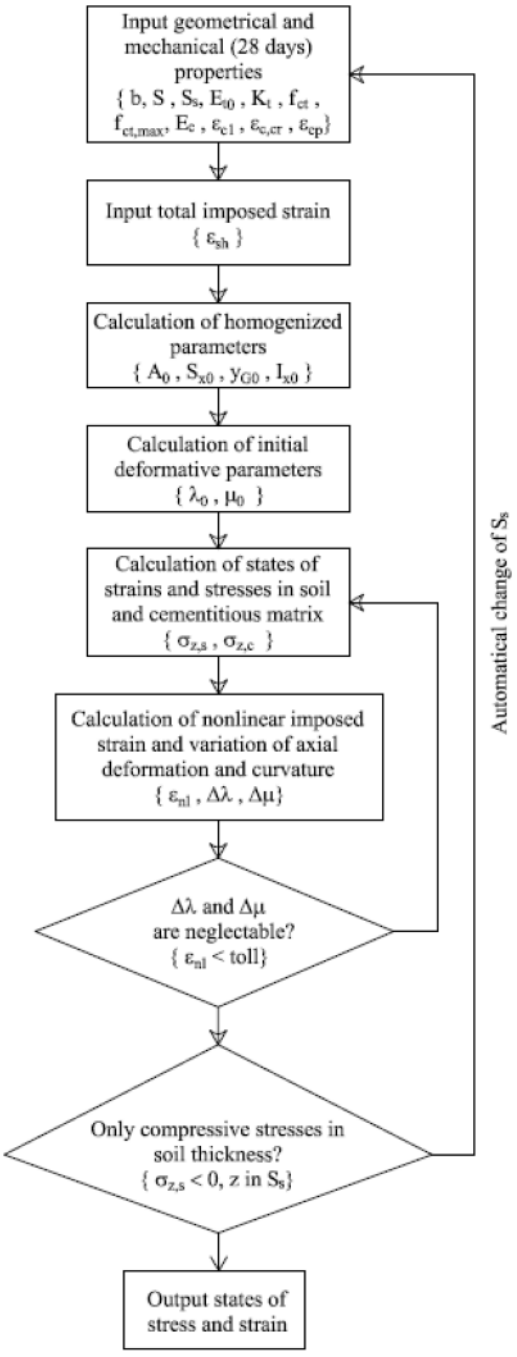

Figure 8. Flowchart of the proposed model.

Table 1. Mechanical properties of the soil.

E_{t0} (MPa)	5000
K_t (MPa/mm)	5

Table 2. Mechanical properties of concrete and HPFRC.

	slab_1	slab_2
b (mm)	5000	5000
S (mm)	100	100
Cement class	32.5N	42.5R
Rck (MPa)	37	50
f_{ck} (MPa)	30	40
E_{cm} (MPa)	33000	36300
f_{ct} (MPa)	2.00	2.50
$f_{ct,max}$ (MPa)	2.00	3.00
$\varepsilon_{c,cr}$ (‰)	0.06	0.07
ε_{cp} (‰)	0.06	2.00
ε_{cu} (‰)	3.5	3.5

(RH = 50%) for 28 days. In this period, the shrinkage is assumed to be the only external action on the slab.

The dashed curves reported in Figure 9a and 9b show the maximum tensile strains reached in the slab_1 and slab_2, respectively. More precisely, these strains are calculated after considering three different distributions of shrinkage (Tiberti et al. 2018). In the same figures, the maximum strain capacity of the cement-based materials is also reported.

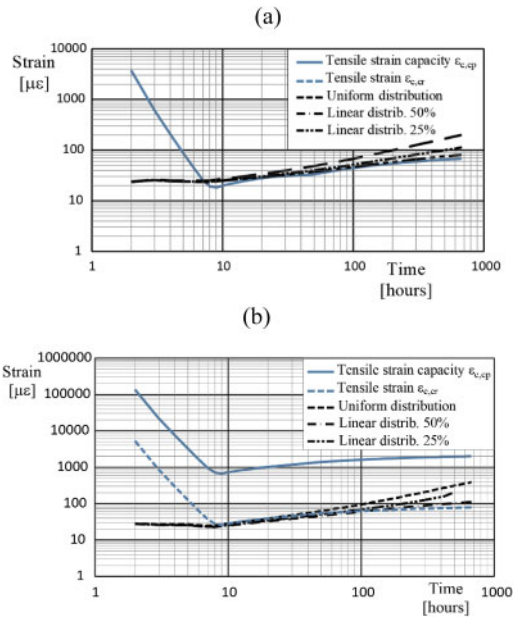

Figure 9. Numerical outcomes in case of (a) slab_1 (C30/37) and (b) slab_2 (HPFRC).

Figure 9a is representative of a concrete that produces a crack 7 hours after casting (i.e., when the strain capacity of concrete is the lowest). In this situation the presence of joints is necessary. In the case of HPFRC (see Figure 9b), due to the absence of crack localization, contraction joints may be avoided.

Nevertheless, in both the slabs, the bi-logarithmic diagrams do not show remarkable variation of tensile

strains with the shrinkage distribution. On the contrary, numerical results show that the most important parameters to obtain jointless slabs on ground are the tensile properties, especially the strain capacity, and shrinkage evolutions (both autogenous and drying).

5 CONCLUSION

Tensile strain capacity of the cementitious matrix is important for designing jointless slabs, and controlling crack widths after strain localization, as well. Current methods for the characterization of tensile properties in concrete and FRC cannot be extended to HPFRC, because in the latter strain localization in tension does not occur at cracking (enhanced capacity). At the same time, mechanical models devoted to the analysis of conventional reinforced concrete (or FRC) slabs on ground behave differently than those made with HPFRC. Hence, a new model for designing jointless slab on ground, made with HPFRC (i.e., a strain hardening material) has been proposed. Based on the results of the analyses previously described, it can be observed that to avoid shrinkage cracking few hours after casting, it is of fundamental importance to know the mechanical properties of cement-based materials at very early age. Specifically, the evolutions of tensile strengths and strains with time are the most significant parameters, like the shrinkage actions. If the tensile strain capacity increases, as in the case of HPFRC, the jointless slabs can be built.

REFERENCES

AASHTO, 1993. AASHTO Guide for design of pavement structures". America.

ACI 209R-92: Prediction of Creep, Shrinkage, and Temperature Effects in Concrete Structures, American Concrete Institute, Farmington Hills, 1997.

Al-Saleh, S. A. 2014. Comparison of theoretical and experimental shrinkage in concrete. Constr. Build. Mater., volume 72: 326–332. The Netherlands: Elsevier.

Bazant, Z.P. & Baweja, S. 2001. Creep and Shrinkage Prediction Model for Analysis and Design of Concrete Structures: Model B3," ACI Special Publications, volume 194: 1-84. USA: ACI Material Journal.

Bentur, A. 2003. Early-age Cracking in Cementitious Systems. RILEM Technical Committee 181-EAS: Early-age Shrinkage Induced Stresses and Cracking in Cementitious Systems. France: RILEM.

Boshoff, W.P. 2012. Plastic Shrinkage Cracking of Concrete, Part 2: Commentary. Report number: ISI2012-17. Germany: Insitute of Structural Engineering.

Burger, A.F 2010. Experience with the construction of an ultrathin continuously reinforced concrete pavement. 11th International Symposium on concrete roads.

Choi, J. & Chen, R. H. L. 2005. Design of Continuously Reinforced Concrete Pavements Using Glass Fiber Reinforced Polymer Rebars. U.S. Department of transportation FHA. America.

ChunPing, G. & Guang, Y. & Wei, S. 2015.Ultrahigh performance concrete–properties, applications and perspectives". Volume 58: 587-599. China: Technological Sciences.

Colonnetti, G. 1950. Elastic equilibrium in the presence of permanent set. Quarterly of applied mathematics Vol. VII No.4: 353-362. https://doi.org/10.1090/qam/33732

Combrinck, R. & Boshoff, W. P. 2019. Tensile properties of plastic concrete and the influence of temperature and cyclic loading. Cement and Concrete Composites, volume 97: 300-311. The Netherlands: Elsevier.

Destrée, X. & Yao, Y. & Mobasher, B. & Asce, M. 2016. Sequential Cracking and Their Openings in Steel-Fiber-Reinforced Joint-Free Concrete Slabs. J. Mater. Civ. Eng., volume 28: (04015158) 1-11. USA: ASCE.

Esser J., Guerini A, Volpatti G, Zampini D. 2015. Advanced fiber reinforced concrete mix designs and admixtures systems, Patent EP3307692 B1 [priority 2015-06-11]. Commercially available as CEMEX®Resilia®.

Eurocode 2: Design of concrete structures – Part 1-1 : General rules and rules for buildings. 2004.

FHA – U.S. Department of transportation, 2019. Technical Advisory: Concrete Pavement Joints. America.

fib Model Code for Concrete Structures 2010 –.

Gardner, N.J. & Lockman, M.J. 2001. Design provisions for drying shrinkage and creep of normal strength concrete. ACI, volume 98: 159-167. USA: ACI Material Journal.

Graybeal, B. F.2013. Development of a Direct Tension Test Method for UHPFRC. ACI Mater J, volume 110: 177-186. USA: 2013.

Gribniak, V. & Kaklauska, G. & Bacinskas, D. & Sung, W. & Sokolov, A. & Ulbinas, D 2011. Investigation of shrinkage of concrete mixtures used for bridge construction in Lithuania. Volume 6: 7-83. Lithuania: The Baltic Journal of Road and Bridge Engineering.

Gűneyisi, E. & Gesoglu, M. & Mohammedameen, A. 2014. Enhancement of shrinkage behavior of lightweight aggregate concretes by shrinkage reducing admixture and fiber reinforcement. Construction and Building Materials, volume 54: 91-98. The Netherlands: Elsevier.

Hachiya, N. J. K. S. 2006. Applicability of concrete with high flexural strength to airport pavements. 10th International Symposium on Concrete Roads.

Hammer, T. & Bjontegaard, O. & Fossa, K. 2007. Cracking tendency of HSC :Tensile strength and self-generated stress in the period of setting and early hardening. Materials and Structures Journal, volume 40: 319-324. The Netherlands: Springer.

Heath, A.C. & Roesler, J.R. 1999. Shrinkage and Thermal Cracking of Fast Setting Hydraulic Cement Concrete Pavements in Palmdale. California.

Larrard, F. & Sedran, T. 2011. High and ultra-High performance concrete in pavement :tools for the road eternity. France: Hal.

R., A.-T. 2009. Renewal of concrete slabs using high performance concrete. 9th International Symposium on concrete roads.

Ramadoss, K. N. P. 2008. Tensile strength and durability characteristics of high-performance fiber reinforced concrete. Arabian J Sci Eng, vol. 33 : 307-319. Saudi Arabia: Springer.

Rasmussen, R.O. & McCullough, B.F. 1998. A Foundation for High Performance Jointed Concrete Pavement Design and Construction Guidelines; Transtec Consultants: Austin, TX. USA.

Rasmussen, R.O. & Rogers, R. & Ferragut, T. R. 2009. Continuously reinforced concrete pavements – Design & Construction guidelines. U.S. Department of transportation FHA. America.

Roesler, J. R. & Hiller, J. E. & Brand, A. S. 2016. Continuously Reinforced Concrete Pavement Manual – Guidelines for Design, Construction, Maintenance, and

Rehabilitation. U.S. Department of transportation FHA. America.

Roziere, E. R. & Cortas, R. & Loukili, A. 2015. Tensile behaviour of early age concrete: New methods of investigation", Cement & Concrete Composites, volume 55: 153-161. The Netherlands: Elsevier.

S. J. CHOI, S. Y. & Park, J. S. & Jung, W. T. 2011. A Study on the Shrinkage Control of Fiber Reinforced Concrete Pavement. Procedia Engineering, Volume 14:2815–2822. The Netherlands: Elsevier.

Savino, V. & Lanzoni, M. & Tarantino A. M. & Viviani, M. 2018. Simple and effective models to predict the compressive and tensile strength of HPFRC as the steel fiber content and type changes. Composites Part B: Engineering, volume 137: 153-162. The Netherlands: Elsevier.

Söderqvist, J. 2006. Design of Concrete Pavements – Design Criteria for Plain and Lean Concrete. Stockholm: licentiate thesis.

Tehmina, A. & Shafiq, N. & Nuruddin, M. 2014. Mechanical Properties of High-Performance Concrete Reinforced with Basalt Fibers. Procedia Engineering, volume 77: 31-139. The Netherlands: Elsevier.

Tiberti, G. & Mudadu, A. & Barragan, B. & Plizzari, G. 2018. Shrinkage Cracking of Concrete Slabs-On-Grade: A Numerical Parametric Study. MDPI Journal Fibers, volume 6:, 64., 2018.

Yoo, D. & Kim, M. & Kim, S. & Ryu, G & Koh, K. 2018. Effects of mix proportion and curing condition on shrinkage behavior of HPFRCCs with silica fume and blast furnace slag. Construction and Building Materials, volume 166: 241-256. The Netherlands: Elsevier.

Yoo, D. & Min, K. & Yoon, Y. 2014. Shrinkage and cracking of restrained ultra-high-performance fiber-reinforced concrete slabs at early age. Construction and Building Materials, volume 73: 357-365. The Netherlands: Elsevier.

Zhang, J. & Wang, Z. & Ju, X. 2013. Application of ductile fiber reinforced cementitious composite in jointless concrete pavements. Composites Part B: Engineering, Volume 50: 224-231. The Netherlands: Elsevier.

Zhang, M. & Leow, M.P. 2003. Effect of water-to-cementitious materials ratio and silica fume on the autogenous shrinkage of concrete. Cement and Concrete Research, volume 10: 687–1694. The Netherlands: Elsevier.

Zhang, M. & Zakaria, M. & Hama, Y. 2013. Influence of aggregate materials characteristics on the drying shrinkage properties of mortar and concrete. Construction and Building Materials, volume 49:500-510. The Netherlands: Elsevier.